

The Optical Gravitational Lensing Experiment. Catalog of stellar proper motions in the OGLE-II Galactic bulge fields

T. Sumi¹, X. Wu¹, A. Udalski², M. Szymański², M. Kubiak², G. Pietrzyński^{2,3},
I. Soszyński², P. Woźniak⁴, K. Żebruń², O. Szewczyk² & L. Wyrzykowski²

¹ Princeton University Observatory, Princeton, NJ 08544-1001, USA; e-mail: (sumi, xawn)@astro.princeton.edu

² Warsaw University Observatory, Al. Ujazdowskie 4, 00-478 Warszawa, Poland;
e-mail: (udalski,msz,mk,pietrzyn,soszynsk,zebrun,szewczyk,wyrzykow)@astrowu.edu.pl

³ Universidad de Concepción, Departamento de Física, Casilla 160-C, Concepción, Chile

⁴ Los Alamos National Laboratory, MS-D436, Los Alamos, NM 87545 USA; e-mail: wozniak@lanl.gov

Accepted Received in original form

ABSTRACT

We present a proper motion (μ) catalogue of 5,080,236 stars in 49 Optical Gravitational Lensing Experiment II (OGLE-II) Galactic bulge (GB) fields, covering a range of $-11^\circ < l < 11^\circ$ and $-6^\circ < b < 3^\circ$, the total area close to 11 square degrees. The proper motion measurements are based on 138 – 555 *I*-band images taken during four observing seasons: 1997–2000. The catalogue stars are in the magnitude range $11 < I < 18$ mag. In particular, the catalogue includes Red Clump Giants (RCGs) and Red Giants in the GB, and main sequence stars in the Galactic disc. The proper motions up to $\mu = 500$ mas yr⁻¹ were measured with the mean accuracy of $0.8 \sim 3.5$ mas yr⁻¹, depending on the brightness of a star. This catalogue may be useful for studying the kinematic of stars in the GB and the Galactic disk.

Key words: Galaxy:bulge – Galaxy:center – Galaxy:kinematics and dynamics – Galaxy:structure – astrometry

1 INTRODUCTION

The Galactic Bulge (GB) is the nearest bulge in which individual stars can be studied in detail. A study of stellar populations and stellar dynamics in the Bulge may help us understand how bulges formed, what are their populations, gravitational potential and structure.

The proper motions with precise photometry might make it possible to separate the observed populations based on their kinematics. Such study has first been done by Spaenhauer, Jones & Whitford (1992) with photographic plates only for a few hundred of brightest red giants in Baade’s window. Recently deeper study has been done by Kuijken & Rich (2002) with *Hubble Space Telescope* (HST)/WFPC2 in Baade’s window.

Several groups have carried out gravitational microlensing observations toward dense stellar fields, such as the Magellanic clouds, the Galactic center and disc. Until now, hundreds of events have been found (EROS: Aubourg et al. 1993; OGLE: Udalski et al. 2000; Woźniak et al. 2001; MACHO: Alcock et al. 2000; MOA: Bond et al. 2001; Sumi et al. 2003), and thousands are expected in the up-

coming years by MOA¹, OGLE-III² and other collaborations.

It is well known that the gravitational microlensing survey data is well suited for numerous other scientific projects (see Paczyński 1996; Gould 1996). The studies of the Galactic structure certainly benefit from this type of data. The microlensing optical depth probes the mass density of compact objects along the line of sight and the event time-scale distribution is related to the mass function and kinematics of the lensing objects. Observed high optical depth may be explained by the presence of the bar (Udalski et al. 1994; Alcock et al. 1997, 2000; Sumi et al. 2003; Afonso et al. 2003; Popowski et al 2003) There is substantial evidence that the Galaxy has a bar at its center (de Vaucouleurs 1964; Blitz & Spergel 1991; Stanek et al. 1994, 1997; Kiraga & Paczyński 1994; Häfner et al. 2000). However, the parameters of the bar, e.g., its mass, size, and the motion of stars within it, still remain poorly constrained.

Stanek et al. (1997) used the Red Clump Giants (RCGs) to constrain the axial ratios and orientation of

¹ <http://www.phys.canterbury.ac.nz/~physib/alert/alert.html>

² <http://www.astrowu.edu.pl/~ogle/ogle3/ews/ews.html>

the Galactic bar. These stars are the equivalent of the horizontal branch stars for a metal-rich population, i.e., relatively low-mass core helium burning stars. RCGs in the GB occupy a distinct region in the colour magnitude diagram (Stanek et al. 2000 and references therein). The intrinsic width of the luminosity distribution of RCGs in the GB is small, about 0.2 mag (Stanek et al. 1997; Paczyński & Stanek 1998). Their observed peak and width of the luminosity function are related to the distance and radial depth of the bar.

Furthermore, Mao & Paczyński (2002) suggested that there should be a difference in average proper motions of 1.6 mas yr^{-1} between the bright and faint RCG sub-samples, which are on average on the near and the far side of the bar, respectively, if their tangential streaming motion is 100 km s^{-1} . Following this suggestion, Sumi, Eyer & Woźniak (2003) measured mean proper motion of bright and faint RCGs in one OGLE-II field in Baade’s Window, and they found a difference to be $1.5 \pm 0.11 \text{ mas yr}^{-1}$.

To expand this analysis we measured proper motions in all 49 GB fields observed by the Optical Gravitational Lensing Experiment³ II (OGLE-II; Udalski et al. 2000) for stars down to $I = 18$ mag, which is sufficiently deep to include RCGs. There are several earlier proper motion catalogues of this general area (c.f. USNO-B:Monet et al. 2002, Improved NLTT:Salim & Gould 2003 and Tycho-2:Høg et al. 2000). Though the area covered by our catalogue is relatively small, it reaches deeper and covers a wide range of proper motion ($\mu < 500 \text{ mas yr}^{-1}$) with the accuracy as good as ($\sim 1 \text{ mas yr}^{-1}$). In §2 we describe the data. We present the analysis method in §3 and 4. In §5, 6 and 7 we describe the property, zero point and problems in our catalogue. Discussion and conclusion are given in §8.

2 DATA

We use the data collected during the second phase of the OGLE experiment, between 1997 and 2000. All observations were made with the 1.3-m Warsaw telescope located at the Las Campanas Observatory, Chile, which is operated by the Carnegie Institution of Washington. The “first generation” camera has a SITe 2048 \times 2048 pixel CCD detector with pixel size of 24 μm resulting in 0.417 arcsec/pixel scale. Images of the GB fields were taken in drift-scan mode at “medium” readout speed with the gain 7.1 e^-/ADU and readout noise of 6.3 e^- . A single 2048 \times 8192 pixel frame covers an area of 0.24 \times 0.95 deg^2 . Saturation level is about 55,000 ADU. Details of the instrumentation setup can be seen in Udalski, Kubiak & Szymański (1997).

In this paper we use 138-555 I -band frames of the BUL_SC1-49 fields. The centers of these fields are listed in Table 1. The time baseline is almost 4 years. There are gaps between the observing seasons when the GB cannot be observed from the Earth, each about 3 months long. The median seeing is $\sim 1.3''$. We use the VI photometric maps of the standard OGLE template (Udalski et al. 2002) as the astrometric and photometric references.

Only about 70% of the area of the BUL_SC1 field overlaps with the extinction map made by Stanek (1996). The extinction map covering all OGLE-II fields has been constructed by Sumi (2003).

3 ANALYSIS

The analysis in this work follows Sumi, Eyer & Woźniak (2003), except our procedure makes it possible to detect high proper motions, extends to the limiting magnitude down to $I = 18$ mag and corrects the systematic effects. The standard OGLE template given by Udalski et al. (2002) serves as the fixed astrometric reference in our analysis. In order to treat properly frame distortions in the y -axis (declination) due to drift-scan mode of observation each OGLE-II field is divided into 64 subframes before processing. Subframes are 2048 \times 128 pixels with a 14 pixel margin on each side.

We compute the pixel positions of stars in the images using the DoPHOT package (Schechter, Mateo & Saha 1993). At the start of the processing for each exposure, the positions of stars in a single subframe are measured and cross-referenced with those in the template and the overall frame shift is obtained. Using this crude shift we can identify the same region of the sky (corresponding to a given subframe of the template) throughout the entire sequence of frames.

To treat properly spatial PSF variations, each 2048 \times 128 pixel subframe is divided into 4 smaller chunks with a size of 512 \times 128 pixels with a 14 pixel margin on each side. Then the positions of stars in all chunks are computed by DoPHOT. We use all stars with $I \leq 18$ mag (~ 400 of them, depending on the stellar density in each field) categorized by DoPHOT as isolated stars (marked as type=1) in the following analysis. We do not use the data points categorized by DoPHOT as a star blended with other stars (marked as type=3).

The stars in each of the chunks are combined into the original 2048 \times 128 subframes. We cross-reference the stars in the template and other frames with a search radius of 0.5 pixels and derive the local transformation between these pixel coordinate systems for each subframe. We use a first order polynomial to fit the transformation. The resulting piece-wise transformation adequately converts pixel positions to the reference frame of the template. Typical residuals are at the level of 0.08 pixels for bright stars ($I < 16$) and 0.2 pixels for all stars ($I < 18$).

By using these transformation matrices, we cross-reference the stars in the template and other frames with a search radius of 1.0 pixels instead of 0.5 pixels used in Sumi, Eyer & Woźniak (2003) to increase the range of detectable high proper motion objects. We estimate that the probability of the mis-identification in this search radius is negligible (0.26 %).

We have found that there are systematic differences in the mean positional shifts of stars from the template position $\langle dx \rangle$ and $\langle dy \rangle$ depending on time and pixel coordinate in x . We have measured the $\langle dx \rangle$ and $\langle dy \rangle$ of the stars in 81 strips ($X = 0 \sim 80$) centered at equal intervals in x coordinate between $0 \leq x \leq 2048$ with a width of ± 25 pixels. Each strip contains typically $\sim 2,000$ stars. In the upper panel of Fig. 1 we show $\langle dx \rangle$ as a function of time for the strip $X = 40$ ($x = 1024 \pm 25$ pixels) in BUL_SC2. We can see

³ see <http://www.astrouw.edu.pl/~ogle> or <http://bulge.princeton.edu/~ogle>

Table 1. Center positions of OGLE-II 49 fields. The number of frames N_f and stars N_s , and the mean of uncertainty in proper motion, $\langle \sigma_\mu \rangle$ (mas yr $^{-1}$), are given as a function of I (mag) for each field. σ_μ is averaged over $I \pm 0.5$ mag.

field	α_{2000}	δ_{2000}	l (deg.)	b (deg.)	N_f	N_s	$\langle \sigma_\mu \rangle$ (mas yr $^{-1}$), for I (mag) =							
							11.5	12.5	13.5	14.5	15.5	16.5	17.5	
BUL_SC1	18 ^h 02 ^m 32.5 ^s	-29°57'41"	1.08	-3.62	259	120697	2.38	0.92	0.88	0.99	1.34	2.53	6.01	
BUL_SC2	18 ^h 04 ^m 28.6 ^s	-28°52'35"	2.23	-3.46	264	140398	2.62	0.94	0.89	1.04	1.40	2.83	6.76	
BUL_SC3	17 ^h 53 ^m 34.4 ^s	-29°57'56"	0.11	-1.93	555	167580	1.98	0.66	0.63	0.78	1.22	2.02	4.66	
BUL_SC4	17 ^h 54 ^m 35.7 ^s	-29°43'41"	0.43	-2.01	514	179906	2.34	0.69	0.69	0.89	1.44	2.50	5.73	
BUL_SC5	17 ^h 50 ^m 21.7 ^s	-29°56'49"	-0.23	-1.33	392	113793	1.95	0.78	0.74	0.84	1.12	2.03	3.54	
BUL_SC6	18 ^h 08 ^m 03.7 ^s	-32°07'48"	-0.25	-5.70	306	65578	1.78	0.92	0.85	0.94	1.25	2.23	4.47	
BUL_SC7	18 ^h 09 ^m 10.6 ^s	-32°07'40"	-0.14	-5.91	323	62357	2.00	0.93	0.90	1.00	1.30	2.27	4.40	
BUL_SC8	18 ^h 23 ^m 06.2 ^s	-21°47'53"	10.48	-3.78	289	52549	2.05	0.90	0.86	0.95	1.20	1.99	3.79	
BUL_SC9	18 ^h 24 ^m 02.5 ^s	-21°47'55"	10.59	-3.98	288	51274	1.82	0.90	0.85	0.91	1.17	1.96	3.71	
BUL_SC10	18 ^h 20 ^m 06.6 ^s	-22°23'03"	9.64	-3.44	291	57064	1.80	0.99	0.93	0.97	1.27	2.13	4.09	
BUL_SC11	18 ^h 21 ^m 06.5 ^s	-22°23'05"	9.74	-3.64	280	51181	1.87	1.01	0.93	0.96	1.24	2.01	3.83	
BUL_SC12	18 ^h 16 ^m 06.3 ^s	-23°57'54"	7.80	-3.37	294	79162	2.26	0.98	0.93	1.02	1.36	2.37	4.71	
BUL_SC13	18 ^h 17 ^m 02.6 ^s	-23°57'44"	7.91	-3.58	270	79082	2.21	1.04	1.02	1.07	1.47	2.50	4.93	
BUL_SC14	17 ^h 47 ^m 02.7 ^s	-23°07'30"	5.23	2.81	290	90091	2.39	1.01	0.97	1.05	1.44	2.41	5.23	
BUL_SC15	17 ^h 48 ^m 06.9 ^s	-23°06'09"	5.38	2.63	285	84372	2.19	0.98	0.94	1.03	1.39	2.26	4.88	
BUL_SC16	18 ^h 10 ^m 06.7 ^s	-26°18'05"	5.10	-3.29	277	100885	2.30	1.01	0.93	1.03	1.42	2.57	5.49	
BUL_SC17	18 ^h 11 ^m 03.6 ^s	-26°12'35"	5.28	-3.45	284	101955	2.21	0.95	0.92	1.02	1.40	2.58	5.50	
BUL_SC18	18 ^h 07 ^m 03.5 ^s	-27°12'48"	3.97	-3.14	275	133282	2.48	0.97	0.91	1.08	1.47	2.91	6.64	
BUL_SC19	18 ^h 08 ^m 02.4 ^s	-27°12'45"	4.08	-3.35	273	112421	2.39	0.97	0.93	1.02	1.38	2.53	5.84	
BUL_SC20	17 ^h 59 ^m 19.1 ^s	-28°52'55"	1.68	-2.47	316	169423	2.70	0.99	0.98	1.15	1.67	3.36	8.10	
BUL_SC21	18 ^h 00 ^m 22.3 ^s	-28°51'45"	1.80	-2.66	321	161268	2.64	0.99	0.96	1.13	1.63	3.34	7.77	
BUL_SC22	17 ^h 56 ^m 47.6 ^s	-30°47'46"	-0.26	-2.95	414	111768	2.32	0.79	0.77	0.83	1.19	1.92	4.59	
BUL_SC23	17 ^h 57 ^m 54.5 ^s	-31°12'36"	-0.50	-3.36	350	94798	2.15	0.80	0.73	0.79	1.10	1.74	4.10	
BUL_SC24	17 ^h 53 ^m 17.9 ^s	-32°52'45"	-2.44	-3.36	359	91733	2.20	0.87	0.80	0.85	1.19	1.88	4.22	
BUL_SC25	17 ^h 54 ^m 26.1 ^s	-32°52'49"	-2.32	-3.56	342	90853	2.48	0.84	0.78	0.86	1.14	1.85	4.30	
BUL_SC26	17 ^h 47 ^m 15.5 ^s	-34°59'31"	-4.90	-3.37	346	95233	2.00	0.85	0.81	0.94	1.31	2.28	5.03	
BUL_SC27	17 ^h 48 ^m 23.6 ^s	-35°09'32"	-4.92	-3.65	334	92508	2.11	0.88	0.84	0.94	1.29	2.22	4.90	
BUL_SC28	17 ^h 47 ^m 05.8 ^s	-37°07'47"	-6.76	-4.42	321	57501	2.15	0.83	0.75	0.79	0.98	1.64	3.43	
BUL_SC29	17 ^h 48 ^m 10.8 ^s	-37°07'21"	-6.64	-4.62	313	57822	2.38	0.81	0.76	0.78	1.00	1.66	3.41	
BUL_SC30	18 ^h 01 ^m 25.0 ^s	-28°49'55"	1.94	-2.84	323	151877	2.65	0.91	0.87	1.05	1.51	2.94	7.05	
BUL_SC31	18 ^h 02 ^m 22.6 ^s	-28°37'21"	2.23	-2.94	334	155383	2.22	0.95	0.92	1.11	1.54	3.11	7.42	
BUL_SC32	18 ^h 03 ^m 26.8 ^s	-28°38'02"	2.34	-3.14	313	155100	2.31	0.93	0.91	1.10	1.55	3.21	7.56	
BUL_SC33	18 ^h 05 ^m 30.9 ^s	-28°52'50"	2.35	-3.66	273	121848	2.57	0.92	0.85	1.00	1.34	2.56	6.01	
BUL_SC34	17 ^h 58 ^m 18.5 ^s	-29°07'50"	1.35	-2.40	329	156281	2.49	0.99	0.95	1.16	1.70	3.04	7.54	
BUL_SC35	18 ^h 04 ^m 28.6 ^s	-27°56'56"	3.05	-3.00	260	139324	2.51	0.96	0.89	1.05	1.45	2.87	6.80	
BUL_SC36	18 ^h 05 ^m 31.2 ^s	-27°56'44"	3.16	-3.20	290	145376	2.70	0.99	0.95	1.10	1.55	3.27	7.92	
BUL_SC37	17 ^h 52 ^m 32.2 ^s	-29°57'44"	0.00	-1.74	406	152704	2.46	0.75	0.72	0.87	1.27	2.13	4.49	
BUL_SC38	18 ^h 01 ^m 28.0 ^s	-29°57'01"	0.97	-3.42	268	123428	2.40	0.93	0.90	1.05	1.43	2.66	6.41	
BUL_SC39	17 ^h 55 ^m 39.1 ^s	-29°44'52"	0.53	-2.21	415	155735	2.46	0.79	0.77	0.91	1.38	2.26	5.53	
BUL_SC40	17 ^h 51 ^m 06.1 ^s	-33°15'11"	-2.99	-3.14	325	82152	2.11	0.89	0.82	0.88	1.19	1.85	3.99	
BUL_SC41	17 ^h 52 ^m 07.2 ^s	-33°07'41"	-2.78	-3.27	312	87013	2.44	0.90	0.86	0.91	1.24	1.96	4.34	
BUL_SC42	18 ^h 09 ^m 05.0 ^s	-26°51'53"	4.48	-3.38	273	99152	2.40	0.98	0.94	1.03	1.45	2.50	5.31	
BUL_SC43	17 ^h 35 ^m 13.5 ^s	-27°11'00"	0.37	2.95	382	76840	1.86	0.80	0.82	0.84	1.14	1.91	3.65	
BUL_SC44	17 ^h 49 ^m 22.4 ^s	-30°02'45"	-0.43	-1.19	343	68457	1.85	0.86	0.86	0.90	1.17	1.98	3.75	
BUL_SC45	18 ^h 03 ^m 36.5 ^s	-30°05'00"	0.98	-3.94	140	107362	3.13	1.67	1.65	1.85	2.45	4.62	10.57	
BUL_SC46	18 ^h 04 ^m 39.7 ^s	-30°05'11"	1.09	-4.14	138	97197	3.38	1.86	1.78	1.94	2.46	4.45	10.43	
BUL_SC47	17 ^h 27 ^m 03.7 ^s	-39°47'16"	-11.19	-2.60	242	47459	3.01	1.32	1.29	1.33	1.59	2.47	4.74	
BUL_SC48	17 ^h 28 ^m 14.0 ^s	-39°46'58"	-11.07	-2.78	237	47673	2.65	1.39	1.29	1.28	1.56	2.44	4.70	
BUL_SC49	17 ^h 29 ^m 25.1 ^s	-40°16'21"	-11.36	-3.25	234	43341	3.09	1.29	1.26	1.25	1.50	2.32	4.51	

the big jump at JD=2451041 (indicated by a vertical dashed line) where the exposure time of OGLE-II in the GB fields has been changed from 87 sec to 99 sec in the middle of 1998 season, on August 15. In the upper panel of Fig. 2 we show typical mean positional shifts in x , $\langle dx \rangle$ of stars in strips in BUL_SC2 as a function of pixel coordinate x . The filled and open circles represent the $\langle dx \rangle$ of the frame taken at JD=2450887.822 (before the jump) and 2451336.769 (after the jump), respectively. There are also systematics in $\langle dy \rangle$ with the level of 0.04 pixels. We cannot see any such sys-

tematics as a function of y pixel coordinate. Because of the good coincidence between the jump and the change in the drift scan rate that determines the effective exposure time, the bulk of the systematics may be caused by the change in drift scan rate. However, we do not know the detail reasons behind this at the present time.

Even within the period before and after the jump, the shapes of Fig. 2 differ from time to time and from field to field at the level of 0.04 pixels. By interpolating these curves of $\langle dx \rangle$ and $\langle dy \rangle$ as a function of x for each frame (time) of

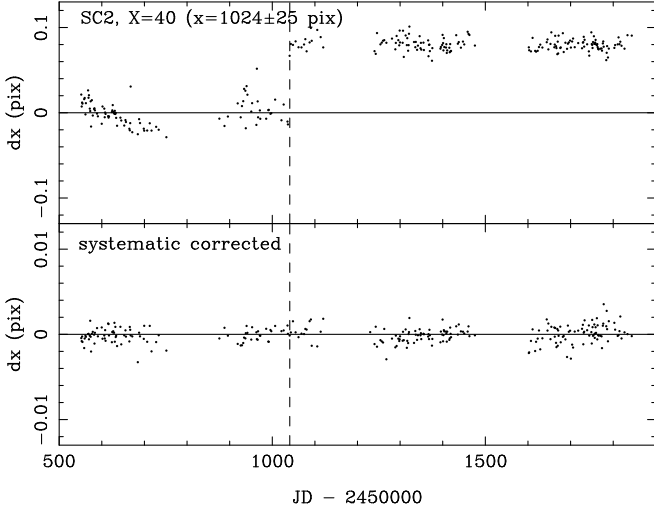


Figure 1. Upper panel: The mean positional shift in x , $\langle dx \rangle$ of stars in a strip $X = 40$ ($x = 1024 \pm 25$ pixels) in BUL_SC2 as a function of time. We can see the big jump at JD=2451041 (indicated by a vertical dashed line) where the exposure time of OGLE-II in the GB fields has changed from 87 sec to 99 sec in the middle of 1998 season, on August 15. Lower panel: The same figure as above after the systematic correction.

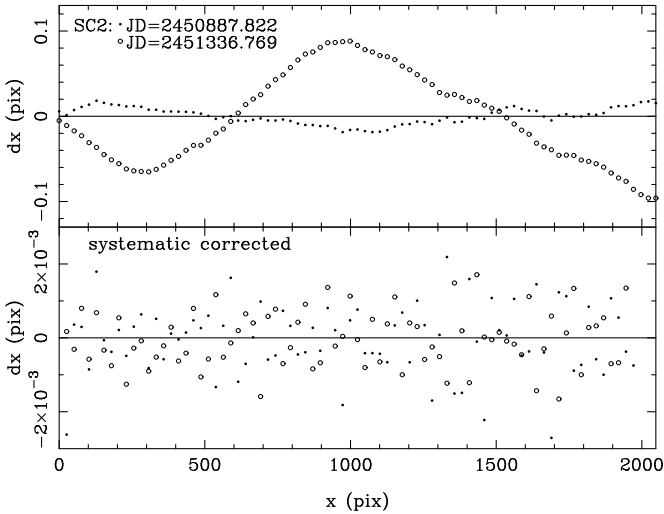


Figure 2. Upper panel: Typical mean positional shifts in x , $\langle dx \rangle$ of stars in strips in BUL_SC2 as a function of pixel coordinate x . The filled and open circles represent the $\langle dx \rangle$ of the frame taken at JD=2450887.822 (before the jump) and 2451336.769 (after the jump), respectively. Lower panel: The same figure as above after the systematic correction. Note that vertical scale in the lower panel is very different than in the upper panel.

each field, we correct dx and dy for each star and frame. In the lower panel of Fig. 1 and Fig. 2, we show the same plots after this systematic correction. This procedure is based on the assumption that average proper motions of a large number of stars in separate groups of columns (i.e. different values of X) should be the same. Note that the integral of the curves shown in Fig. 2 over all x -columns is unity, as this corresponds to the average position of all stars.

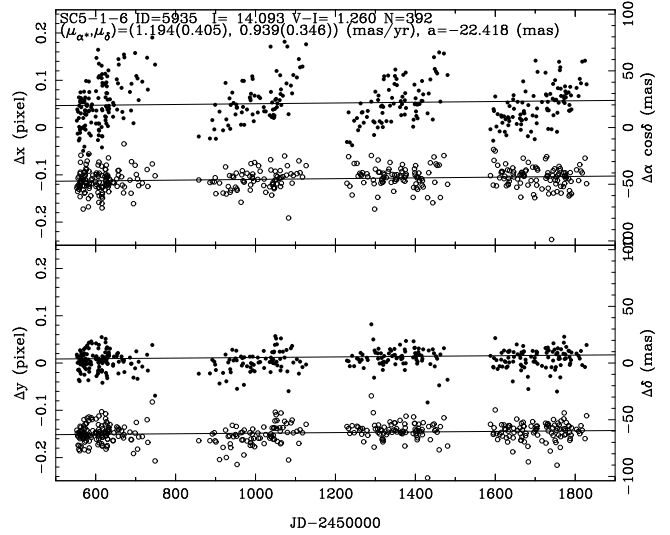


Figure 3. Time variation of the position in $\alpha \cos \delta$ (upper) and δ (lower) for star ID=5935 ($V-I=1.260$) in BUL_SC5. Filled circles represent actual positions, while open circles are positions corrected for differential refraction with an offset of -0.16 pixels. Solid lines indicate a model fit for the proper motion $(\mu_{\alpha*}, \mu_{\delta}) = (-1.19(0.41), 0.94(0.35))$ (mas yr^{-1}) with the 1σ errors in bracket. The differential refraction coefficient is $a = -22.42$ mas.

An example of time dependence of the position for a star with a moderate detectable proper motion is shown in Fig. 3 with filled circles. To measure the proper motions in right ascension ($\mu_{\alpha*} \equiv \mu_{\alpha} \cos \delta$) and in declination (μ_{δ}), we fit the positions as a function of time t with the following formula:

$$\alpha = \alpha_0 + \mu_{\alpha*} t + a \sin C \tan z, \quad (1)$$

$$\delta = \delta_0 + \mu_{\delta} t + a \cos C \tan z, \quad (2)$$

where a is the coefficient of differential refraction, z is the zenith angle, and C is the angle between the line joining the star and Zenith and the line joining the star with the South Pole, and α_0 and δ_0 are constants. The parameter a is a function of the apparent star colour. We neglect the parallactic motion due to the Earth's orbit because its effect is strongly degenerate with the effect of differential refraction for stars in the direction of the GB (Eyer & Woźniak 2001).

In Fig. 3 we present with solid lines and open circles the best fit model for the proper motion $(\mu_{\alpha*}, \mu_{\delta})$ and positions allowing for the differential refraction respectively. As is written in this figure, the parameters for this object are: field SC5-1-6, which means that this object is in the OGLE-II field BUL_SC5, and chunk $(X_{\text{chunk}}, Y_{\text{chunk}}) = (1, 6)$, OGLE ID=5935, $I = 14.093$, $V - I = 1.260$, the number of data points $N = 392$, proper motion $(\mu_{\alpha*}, \mu_{\delta}) = (1.19(0.41), 0.94(0.35))$ (mas yr^{-1}) with 1σ errors in brackets. The differential refraction coefficient is $a = -22.42$ mas.

We computed α_0 , δ_0 , $\mu_{\alpha*}$, μ_{δ} and a for all stars used to transform coordinate systems (approximately the number of fields times the number of chunks times the typical number of stars per chunk, i.e. $49 \times 256 \times 400$). In cases where the star is measured in the overlap region of more than one chunk of a given field, the data set with the largest

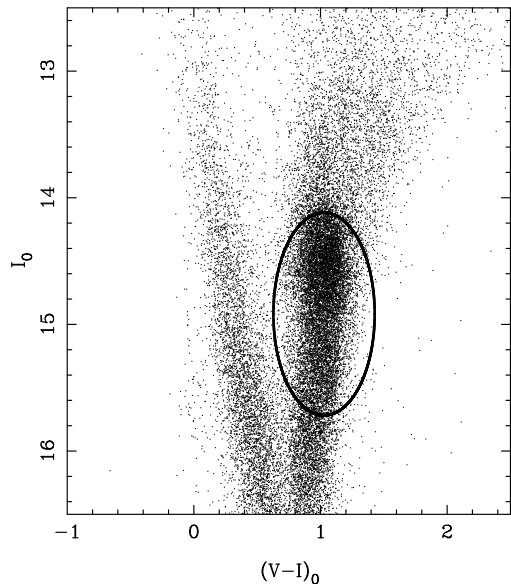


Figure 4. Colour Magnitude Diagram of stars with $\sigma_\mu < 2.5$ mas yr^{-1} in BUL_SC2. I_0 and $(V - I)_0$ are extinction corrected I -band magnitude and $V - I$ colour. The stars in GB are defined within the ellipse centered at the center of RCGs plus 0.4 mag in I .

number of points is selected. Stars with the fewer than 20 data points are rejected. The catalogue of whole BUL_SC1 was recomputed in this analysis because the catalogue presented by Sumi, Eyer & Woźniak (2003) contains only 70 % of this field.

Our catalogue contains 5,080,236 stars, which is 79.8 % of all objects with $I \leq 18$ mag in the original OGLE template (Udalski et al. 2002). 7% of these stars do not have any V -band photometry. The missing V -band photometry of stars can be estimated from the differential refraction coefficient because there is good correlation between the differential refraction coefficient a and the apparent $V - I$ colour for stars (see Fig. 8), provided they belong to the same population as that of the majority.

We have measured the mean proper motions of stars in the Galactic bulge (GB) defined in the ellipse in the Colour Magnitude Diagram (CMD) in Fig. 4, where the extinction and reddening are corrected by using the extinction map of Sumi (2003). The ellipse is located at the center of the RCGs estimated in Sumi (2003) plus 0.4 mag in I and have semi-major and minor axes of 0.9 mag and 0.4 mag, respectively. This ellipse includes RCGs and Red Giants in the GB. Here we chose only objects whose proper motion accuracy is better than 2.5 mas yr^{-1} . These mean proper motions of stars in the GB are assumed to be constant within each field. In Fig. 5 we show these measured mean proper motions of stars in the GB as a function of x (upper panel) and after the systematic correction (lower panel). We can see how well the systematic distortions are corrected. Note that our instrumental reference frame is defined by all stars, and this is why the average proper motion of stars in the GB are not zero.

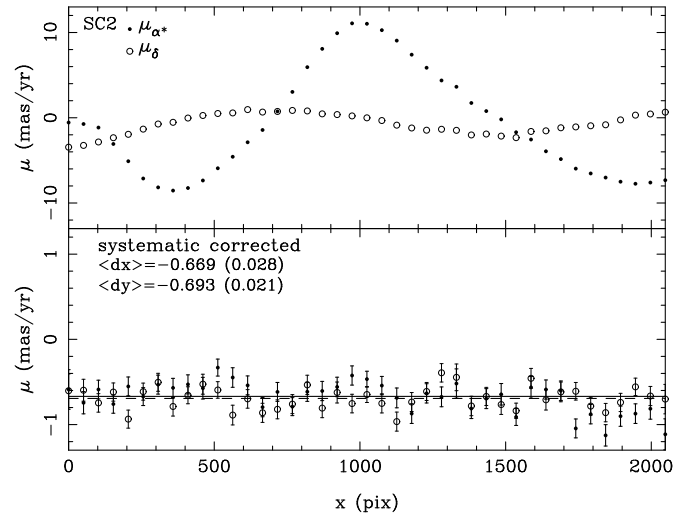


Figure 5. Upper panel: The mean proper motions in x (filled circle) and in y (open circle), for stars in 50 pixels strips in BUL_SC2 as a function of pixel coordinate x . Lower panel: The same figure as above after the systematic correction.

4 HIGH PROPER MOTION OBJECTS

The detectability of high proper motions is limited by the search radius used for cross-identification of stars on all images. The search radius, 1 pix yr^{-1} , corresponds to $\sim 400 \text{ mas yr}^{-1}$. Objects with $\mu \geq 100 \text{ mas yr}^{-1}$ cannot be identified over the full four year long observing interval of OGLE-II, as they move out of the search radius. In order to be able to follow fast moving stars over four observing seasons we made additional astrometry for objects for which preliminary estimates gave a proper motion $\mu \geq 100 \text{ mas yr}^{-1}$. Whenever a star moved more than 0.4 pixels from the previous search center we moved that center to the median location of the last 3 data points. This procedure was adopted when it allowed us to locate the star in a larger number of CCD images.

We show the positional movement of one of the highest proper motion objects in Fig. 6 and images at 1997 and at 2000 in Fig. 7. This star has relatively fewer data points because this star is overexposed on the good seeing frames in the I -band. This star does not have any V -band measurements because of the failure of cross-identification in the V -band template image due to its high proper motion. I -band measurements of such objects may also be unreliable because the OGLE photometric maps are based on the measurements by the "fixed position mode" over years (Udalski et al. 2002). The photometries of this star obtained by hand relative to the neighboring stars are: $I = 11.70$, $V - I = 2.86$. This colour is very red as expected from the relation between differential refraction coefficient a from the fit and colour in Fig. 8, but its a and $V - I$ do not match the relation exactly.

The relation between a and $V - I$ for BUL_SC42 in which the extinctions are relatively small, is slightly different from that for BUL_SC5 plotted in Fig. 8. The zero-point of a is 15 mas higher than that for BUL_SC5, but the expected colour of this star from this relation is still redder ($V - I = 4 - 5$). In these figures the slopes differ between fields for

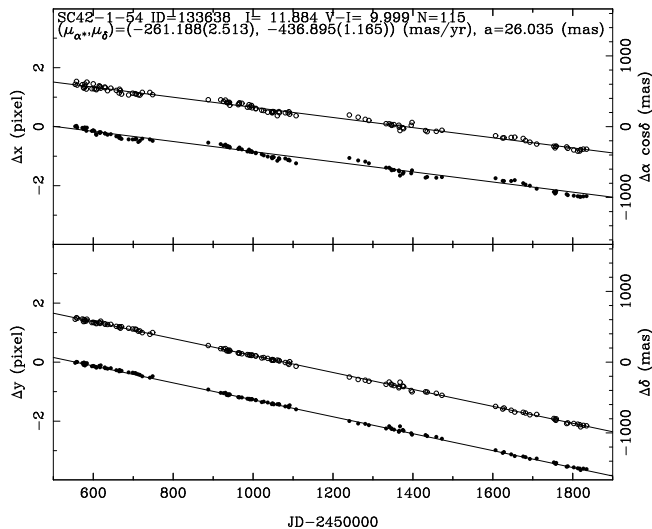


Figure 6. Same plots as Fig. 3 for ID=133638 ($V-I$ =none) in OGLE-II field BUL_SC42, one of the highest proper motion stars. Filled circles represent the actual positions and open circles are the positions corrected for differential refraction, with an offset of +1.5 pixels. Solid lines indicate a model fit for the proper motion $(\mu_{\alpha^*}, \mu_{\delta}) = (-261.19(2.51), -436.90(1.2))$ (mas yr^{-1}) with 1σ errors in bracket. The differential refraction coefficient is $a = 26.04$ mas, which indicates the star is very red. This star does not have V -band magnitude because of the high proper motion. The photometries of the star obtained by hand relatively to the neighboring stars are: $I = 11.70$, $V - I = 2.86$.

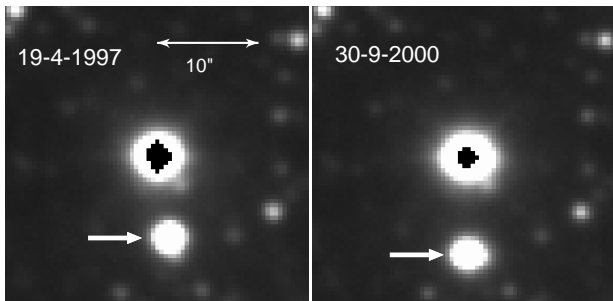


Figure 7. Images of the high proper motion star in Fig. 6, i.e. ID=133638 in OGLE-II field BUL_SC42, at 19 April 1997 (left) and at 30 September 2000 (right).

the region $V - I > 3$. This is because of the difference of the population. In BUL_SC5, the majority in this colour region are RCGs and Red Giant Branch stars, but Red Super Giants in BUL_SC42. So this disagreement might be because this object is a nearby very red dwarf of M4-5 spectral type, not typical for this catalogue.

5 CATALOGUE

A sample for our catalogue of proper motions is shown in Table 2. The complete list of all 5,080,236 stars is available in electronic format via anonymous ftp from the server ftp://ftp.astroww.edu.pl/ogle/ogle2/proper_motion/ and ftp://bulge.princeton.edu/ogle/ogle2/proper_motion/. The list contains star ID, the number μ_{α^*} and μ_{δ} and in

galactic coordinate μ_l and μ_b with their errors, differential refraction coefficient a , standard deviation (Sdev) of data points in the fitting, equatorial coordinates α_{2000} , δ_{2000} in 2000, apparent I -band magnitude and $V - I$ colour, pixel coordinates on CCD x and y , and position of chunk X_c and Y_c to which this object belongs. ID, 2000 coordinates, I and $V - I$ for each object are identical to those in Udalski et al. (2002). If the object doesn't have V -band photometry the $V - I$ colour is written as 9.999.

Note that the number of data points N differs from star to star even if they have similar brightness. This is because some are near the edge of the CCD image or CCD defects, and others are affected by blending. We use the positions which are categorized as a single isolated star by DoPHOT. Hence, blended stars can not be measured when the seeing is poor.

In Fig. 8 we present a colour – magnitude diagram (CMD) for stars in OGLE field BUL_SC5, which is one of the most reddened OGLE-II fields. We also show the correlation between the differential refraction coefficient a and the apparent $V - I$ colour for stars with $I < 16$ in this field. This correlation for other fields is similar, but it has a slight dependence on the population of the majority of stars in each field. In Fig. 9, we plot the uncertainties in μ_{α^*} ($\sigma_{\mu_{\alpha^*}}$, upper panel), in μ_{δ} ($\sigma_{\mu_{\delta}}$, middle panel) and difference between them ($\sigma_{\mu_{\alpha^*}} - \sigma_{\mu_{\delta}}$, lower panel) in BUL_SC3 as a function of the apparent I -band magnitude. In the lower panel, where open circles represent mean values for each 1 magnitude bin, we can see that $\sigma_{\mu_{\alpha^*}}$ is systematically larger than $\sigma_{\mu_{\delta}}$ at $\sim 0.1 \text{ mas yr}^{-1}$ level. We see the same trend in all our fields. This trend is expected from the residual scattering due to the systematic correction and the differential refraction which is large in the direction of α . The mean uncertainties $\langle \sigma_{\mu} \rangle \equiv \langle \sqrt{\sigma_{\mu_{\alpha^*}}^2 + \sigma_{\mu_{\delta}}^2} \rangle$ with 2σ clipping as a function of I are listed in Table 1. Note: that the accuracy of proper motions in our catalogue is better than 1 mas yr^{-1} for $12 < I < 14$.

Fig. 10 shows the histogram of our proper motion measurements μ for the whole catalogue, with the lines with increasing thickness corresponding to all stars, and to those with the proper motion detected with confidence better than 3σ , 5σ and 10σ , respectively. The total number of stars with proper motions measured to 3σ , 5σ and 10σ accuracy is $N_3 = 1,469,838$, $N_5 = 568,665$, $N_{10} = 61,231$, respectively. The inclined solid line: $(\log(N) = -3\log(\mu) + \text{const.})$, has a slope corresponding to the expectation for a uniform distribution and kinematics of stars in space. The distribution of accurate (5σ and 10σ) proper motions seems to be roughly consistent with the uniform distribution.

However, the number of very high proper motion stars, ($\mu > 200 \text{ mas yr}^{-1}$), appears to be smaller than expected from a uniform distribution. This may be due to saturation of images of nearby, and therefore apparently bright, stars in OGLE images.

The distribution of less accurate ($\leq 3\sigma$) proper motions has an apparent cut-off at $\mu \sim 100 \text{ mas yr}^{-1}$. Such stars are apparently faint, their positions have large errors, and they may be difficult to identify in a search radius of 1 pixel, which corresponds to $\mu \sim 100 \text{ mas yr}^{-1}$.

A more thorough analysis of various selection effects is beyond the scope of this paper. Readers are advised to use caution in a statistical analysis of our catalogue.

Table 2: Sample of proper motion catalogue for BUL_SC2.

ID	N	$\mu_{\alpha*}$	$\sigma_{\mu_{\alpha*}}$	μ_{δ}	$\sigma_{\mu_{\delta}}$ (mas yr ⁻¹)	μ_l	σ_{μ_l}	μ_b	σ_{μ_b}	a	Sdev (mas)	α_{2000} (deg)	δ_{2000} (deg.)	I (mag)	$V - I$	x (pixel)	y (pixel)	X_c	Y_c
13213	203	2.96	0.90	-0.44	0.63	1.06	0.70	-2.80	0.84	0.69	13.02	270.99213	-29.24292	15.282	1.522	62.52	904.72	1	7
13214	258	1.09	0.66	-2.03	0.41	-1.24	0.48	-1.94	0.61	-0.88	10.16	271.03837	-29.24297	15.507	1.716	413.60	904.92	1	8
13215	255	-1.71	0.68	-4.75	1.01	-4.98	0.94	-0.82	0.77	1.18	16.10	271.04729	-29.24297	15.572	1.599	481.45	904.94	1	7
13216	247	-0.11	0.67	-1.46	0.51	-1.33	0.55	-0.62	0.64	-0.57	10.95	271.00104	-29.24281	15.635	1.990	130.10	905.70	1	7
13217	250	-3.44	0.83	-0.74	0.76	-2.32	0.78	2.64	0.81	-2.72	14.72	271.00654	-29.24286	15.768	1.746	171.88	905.41	1	7
13218	264	1.49	1.01	-0.30	0.66	0.46	0.76	-1.45	0.94	-3.97	16.19	271.04246	-29.24286	14.960	1.711	444.59	905.97	1	8
13219	263	-3.31	0.91	-1.75	0.39	-3.14	0.56	2.04	0.82	-2.80	13.20	271.02271	-29.24231	15.132	1.931	294.82	910.42	1	8
13220	247	-1.11	0.78	-4.67	1.41	-4.62	1.29	-1.31	0.97	2.30	20.88	270.99650	-29.24206	15.436	1.644	95.64	912.22	1	8
13222	262	-3.98	0.55	-6.50	0.50	-7.62	0.51	0.31	0.54	0.29	9.87	271.01058	-29.24183	15.310	1.853	202.60	914.42	1	8
13223	245	2.25	1.11	-7.76	1.14	-5.68	1.13	-5.75	1.12	5.67	20.22	271.04275	-29.24197	15.369	1.903	446.73	913.63	1	8
13224	189	-2.72	0.87	0.31	0.64	-1.06	0.70	2.53	0.82	-3.43	12.55	270.99100	-29.24144	15.874	1.915	53.69	917.54	1	8
13225	131	0.83	0.88	-3.41	1.01	-2.57	0.98	-2.39	0.91	1.48	13.38	270.98617	-29.24125	15.460	1.795	17.09	919.06	1	8
13227	248	0.32	0.53	-5.23	0.68	-4.41	0.65	-2.83	0.57	0.41	11.08	271.03579	-29.24092	15.015	1.690	394.10	922.69	1	8
13228	262	0.45	0.60	1.12	0.62	1.20	0.62	0.15	0.61	0.31	11.51	271.00475	-29.24047	15.208	1.909	158.16	926.03	1	8
13229	245	-1.94	0.92	-6.90	0.98	-6.97	0.97	-1.67	0.93	0.10	17.20	270.99608	-29.24036	15.402	1.876	92.42	926.87	1	8
13230	264	3.89	0.57	3.85	0.60	5.26	0.59	-1.52	0.58	-0.14	11.09	271.02446	-29.24042	15.082	1.757	307.89	926.93	1	8
13231	249	0.82	0.76	-0.58	0.68	-0.11	0.70	-1.00	0.74	-1.17	13.26	271.03533	-29.24047	15.090	1.850	390.64	926.65	1	8
13232	200	2.53	1.72	11.04	1.50	10.87	1.56	3.17	1.67	0.86	26.09	271.00042	-29.24025	15.608	1.658	125.33	928.07	1	8

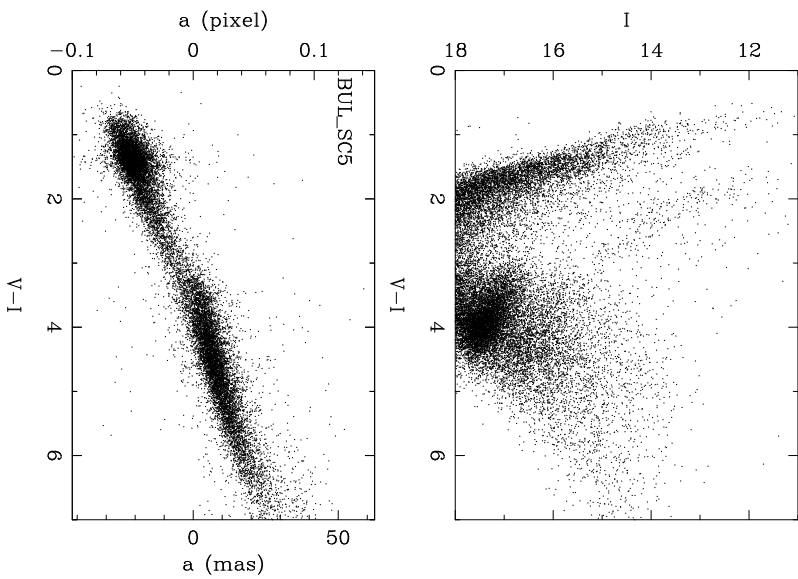


Figure 8. Upper: Colour – magnitude diagram of a quarter of the analyzed stars in OGLE-II field BUL_SC5. Lower: correlation between the differential refraction coefficient a and the apparent colour for stars with $I < 16$ in this field.

6 ZERO POINT

The proper motions in our catalogue are relative values. We need QSOs behind our fields to define the zero point of our proper motions in the inertial frame. However we can get rough information of the zero point of our proper motions by measuring the average proper motion of stars located in the GB, which is presumably close to absolute proper motion of the Galactic Center (GC).

We select stars in the GB defined in Fig. 4. Here we choose only objects whose proper motion accuracy is better than 2.5 mas yr⁻¹. We divide them into bins with a width of $\Delta I = 0.1$ mag in I -band magnitude and take mean of their proper motions for each bin. We plot these mean proper motions ($\mu_{l,b}$) as a function of I for BUL_SC2 in Fig. 11. In this figure we can see the streaming motion of bright ($I \sim 14.1$) and faint ($I \sim 14.7$) RCGs in μ_l . The proper motion of Red Giants ($I > 15$) is the same as the average motion of the RCGs, as expected since Red Giants are on average in the GC.

To measure the proper motion of the GC, $\mu_{l,GC}$ and $\mu_{b,GC}$ in our reference frame, without any bias due to the incompleteness for fainter stars, we take a mean of these $\langle \mu_{l,b} \rangle$ without weighting by their errors. This provides an estimate that is more reliable than taking the mean proper motion of all individual stars. The measured $\mu_{l,GC}$ and $\mu_{b,GC}$ are shown as a solid and dashed line for BUL_SC2 in Fig. 11 and listed for other fields in Table 3 along with those in equatorial coordinates ($\mu_{\alpha*,GC}$, $\mu_{\delta,GC}$). Table 3 is also avail-

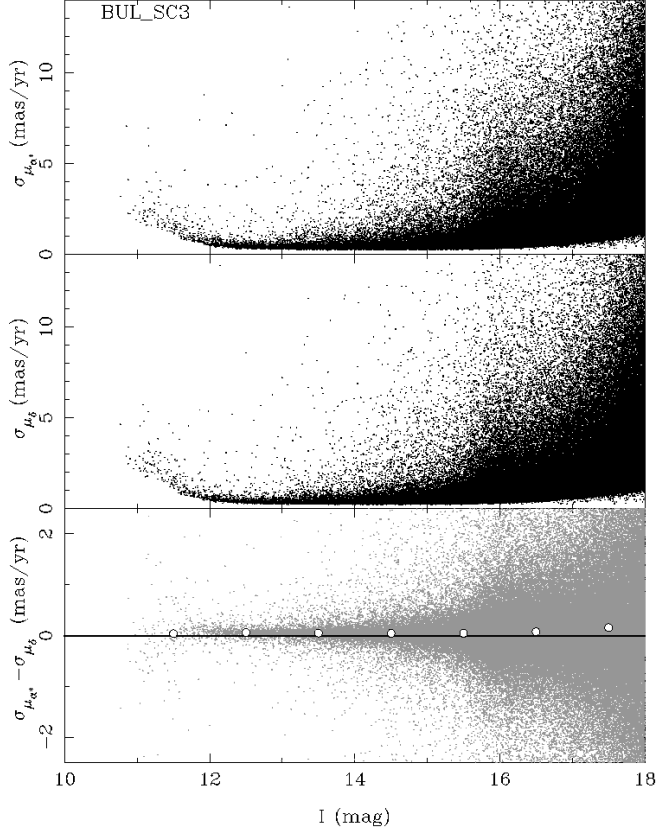


Figure 9. Uncertainties in μ_{α^*} ($\sigma_{\mu_{\alpha^*}}$, upper panel), μ_{δ} ($\sigma_{\mu_{\delta}}$, middle panel) and the difference between them ($\sigma_{\mu_{\alpha^*}} - \sigma_{\mu_{\delta}}$, lower panel) in OGLE-II field BUL_SC3 as a function of the I -band magnitude. In the lower panel, where open circles represent mean values for each 1 magnitude bin, we can see that $\sigma_{\mu_{\alpha^*}}$ is systematically larger than $\sigma_{\mu_{\delta}}$ by $\sim 0.1 \text{ mas yr}^{-1}$ level.

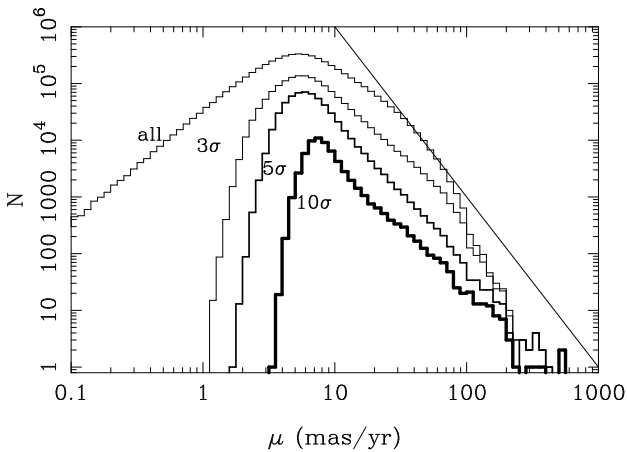


Figure 10. Histograms are shown for μ for all $N = 5,080,236$ stars, and for measurements with confidence better than 3σ , 5σ and 10σ (from the thinnest to the thickest line, respectively) for all 49 OGLE-II fields. The total number of stars with proper motion with 3σ , 5σ and 10σ accuracy are $N_3 = 1,469,838$, $N_5 = 568,665$, $N_{10} = 61,231$. The inclined solid line: $(\log(N) = -3\log(\mu) + \text{const.})$ has the slope expected from stars that have uniform distribution and kinematics.

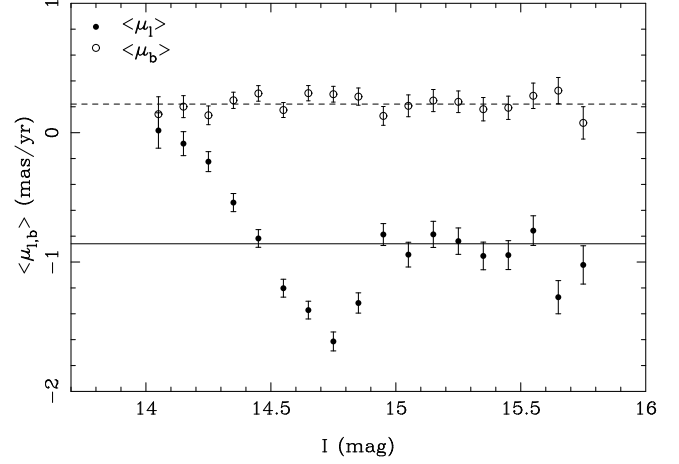


Figure 11. Mean proper motions of stars at GC $\langle\mu_l\rangle$ (filled circle) and $\langle\mu_b\rangle$ (open circle) within $\Delta I = 0.1 \text{ mag}$ bin as a function of I -band magnitude. Solid and dashed lines represent the mean of these bins without weighting by errors. We can see the streaming motion of bright ($I \sim 14.1$) and faint (~ 14.7) RCGs. The proper motion of Red Giants ($I > 15$) is the mid of them as expected from that they are on average on the GC.

able in electronic format via anonymous ftp with the main catalogue (see § 5).

The proper motion measurements in our catalogue can be transformed to the inertial frame by formula;

$$\mu_{\alpha^* \text{OGLE}} = \mu_{\alpha^*} - \mu_{\alpha^*, \text{GC}} + \mu_{\alpha^*, \text{GC, inert}} \quad (3)$$

$$\mu_{\delta \text{OGLE}} = \mu_{\delta} - \mu_{\delta, \text{GC}} + \mu_{\delta, \text{GC, inert}}. \quad (4)$$

Here $(\mu_{\alpha^*, \text{GC, inert}}, \mu_{\delta, \text{GC, inert}}) = (-2.93, -5.17) \text{ mas yr}^{-1}$ is the expected proper motion of the GC relative to the inertial frame, assuming a flat rotation curve of $v_r \sim 220 \text{ km s}^{-1}$, the distance between the GC and the Sun of $R_0 = 8.0 \text{ kpc}$ (Eisenhauer et al. 2003) and Solar velocity of $(v_{\odot l}, v_{\odot b}) = (5.25 \text{ km s}^{-1}, 7.17 \text{ km s}^{-1})$ relative to the Local Standard of Rest (LSR) (Dehnen & Binney 1998). This transformation gives us crude absolute proper motions, while this gives us very good relative zero points from field to field as we show later.

The reader can apply this transformation formula to our catalogue to get value in the inertial frame. We didn't apply this transformation to our catalog because the transformation to the inertial frame can be improved with the QSOs to be discovered behind our fields in the future.

To check our measurements we cross-identified stars in our catalogue with the Tycho-2 catalogue (Høg et al. 2000). We selected from our catalogue objects with proper motions higher than 10 mas yr^{-1} and measured with a significance above 3σ , to avoid mis-identification. Most high proper motion stars in Tycho-2 are saturated in OGLE images. We found 65 Tycho-2 stars in our catalogue and their proper motions: μ_{α^*} (thin) and μ_{δ} (thick) are presented in Fig. 12. Here OGLE proper motions have been transformed into the inertial frame by equations (3) and (4). We can see a very good correlation between OGLE and Tycho-2 measurements. Dashed lines indicate $\mu_{\text{OGLE}} = \mu_{\text{Tycho-2}}$, and solid lines represent best fit with fixed unit slope and a possible

Table 3. Proper motions of the GC for all 49 OGLE-II fields. The number of stars used in measurements N_{star} , proper motions of the GC in our reference frame in equatorial coordinate $\mu_{\alpha,GC}$ and $\mu_{\delta,GC}$ and galactic coordinate $\mu_{l,GC}$ and $\mu_{b,GC}$ with their errors.

field	N_{star}	$\mu_{\alpha,GC}$	$\sigma_{\mu_{\alpha,GC}}$	$\mu_{\delta,GC}$	$\sigma_{\mu_{\delta,GC}}$	$\mu_{l,GC}$	$\sigma_{\mu_{l,GC}}$	$\mu_{b,GC}$	$\sigma_{\mu_{b,GC}}$
BUL_SC1	23938	-0.57	0.07	-0.55	0.11	-0.76	0.12	0.23	0.04
BUL_SC2	25738	-0.61	0.05	-0.64	0.09	-0.86	0.10	0.22	0.02
BUL_SC3	43597	-0.66	0.05	-0.68	0.08	-0.92	0.09	0.22	0.02
BUL_SC4	42847	-0.57	0.06	-0.62	0.10	-0.82	0.11	0.18	0.04
BUL_SC5	12704	-0.72	0.08	-0.94	0.12	-1.18	0.14	0.14	0.05
BUL_SC6	10167	-0.61	0.05	-0.80	0.08	-0.99	0.09	0.15	0.03
BUL_SC7	9431	-0.55	0.06	-0.68	0.10	-0.86	0.11	0.16	0.03
BUL_SC8	7397	-0.98	0.05	-0.97	0.08	-1.31	0.09	0.41	0.04
BUL_SC9	7364	-0.85	0.05	-1.02	0.08	-1.30	0.09	0.28	0.03
BUL_SC10	8476	-0.84	0.06	-0.98	0.11	-1.26	0.12	0.28	0.03
BUL_SC11	8067	-0.80	0.06	-1.03	0.10	-1.28	0.11	0.23	0.03
BUL_SC12	9913	-0.95	0.05	-1.33	0.08	-1.62	0.09	0.20	0.03
BUL_SC13	9899	-0.84	0.06	-1.13	0.10	-1.39	0.11	0.20	0.03
BUL_SC14	19398	-0.57	0.05	-0.70	0.08	-0.89	0.10	0.12	0.01
BUL_SC15	16454	-0.53	0.05	-0.79	0.08	-0.95	0.09	0.04	0.03
BUL_SC16	15801	-0.71	0.06	-1.00	0.09	-1.22	0.10	0.15	0.04
BUL_SC17	16665	-0.68	0.05	-0.97	0.07	-1.18	0.08	0.13	0.04
BUL_SC18	23064	-0.60	0.05	-0.73	0.09	-0.93	0.10	0.17	0.02
BUL_SC19	21441	-0.60	0.05	-0.77	0.08	-0.96	0.09	0.16	0.02
BUL_SC20	31933	-0.42	0.06	-0.61	0.10	-0.74	0.11	0.06	0.04
BUL_SC21	30486	-0.55	0.06	-0.71	0.09	-0.89	0.11	0.13	0.03
BUL_SC22	31278	-0.57	0.05	-0.60	0.08	-0.80	0.10	0.20	0.02
BUL_SC23	27679	-0.59	0.06	-0.70	0.10	-0.91	0.11	0.16	0.02
BUL_SC24	27355	-0.55	0.06	-0.59	0.08	-0.79	0.09	0.18	0.03
BUL_SC25	25782	-0.52	0.05	-0.66	0.09	-0.83	0.10	0.12	0.02
BUL_SC26	21577	-0.62	0.05	-0.66	0.07	-0.88	0.08	0.19	0.02
BUL_SC27	20250	-0.60	0.04	-0.72	0.07	-0.92	0.08	0.15	0.02
BUL_SC28	12159	-0.73	0.05	-0.78	0.07	-1.04	0.07	0.22	0.04
BUL_SC29	11755	-0.75	0.04	-0.78	0.05	-1.06	0.06	0.24	0.02
BUL_SC30	29140	-0.54	0.05	-0.64	0.08	-0.82	0.10	0.15	0.03
BUL_SC31	28389	-0.44	0.06	-0.67	0.10	-0.80	0.11	0.06	0.03
BUL_SC32	25750	-0.53	0.06	-0.65	0.09	-0.82	0.10	0.15	0.03
BUL_SC33	23709	-0.61	0.06	-0.69	0.10	-0.90	0.12	0.20	0.02
BUL_SC34	32041	-0.53	0.06	-0.59	0.09	-0.78	0.11	0.17	0.03
BUL_SC35	25997	-0.56	0.05	-0.66	0.09	-0.85	0.10	0.17	0.03
BUL_SC36	24278	-0.59	0.05	-0.64	0.08	-0.85	0.10	0.21	0.02
BUL_SC37	38711	-0.68	0.06	-0.75	0.09	-0.99	0.10	0.20	0.03
BUL_SC38	25633	-0.46	0.06	-0.64	0.10	-0.79	0.12	0.08	0.03
BUL_SC39	41129	-0.47	0.06	-0.64	0.11	-0.79	0.12	0.08	0.02
BUL_SC40	25729	-0.52	0.05	-0.57	0.08	-0.76	0.10	0.16	0.02
BUL_SC41	25665	-0.50	0.05	-0.56	0.07	-0.74	0.08	0.15	0.03
BUL_SC42	18649	-0.79	0.06	-0.88	0.10	-1.15	0.11	0.26	0.04
BUL_SC43	25012	-0.36	0.07	-0.36	0.11	-0.50	0.13	0.11	0.03
BUL_SC44	—	—	—	—	—	—	—	—	—
BUL_SC45	13776	-0.43	0.08	-0.32	0.14	-0.49	0.15	0.22	0.03
BUL_SC46	12608	-0.40	0.08	-0.23	0.14	-0.40	0.16	0.24	0.04
BUL_SC47	6294	-1.18	0.07	-1.20	0.10	-1.65	0.12	0.31	0.03
BUL_SC48	6965	-1.09	0.06	-1.00	0.08	-1.44	0.10	0.35	0.03
BUL_SC49	6299	-0.99	0.06	-0.86	0.08	-1.26	0.09	0.35	0.04

offset. A good correspondence between Tycho-2 and OGLE-II proper motions gives us certain confidence in our measurements. Slightly larger offsets in μ_{δ} imply that the error in absolute proper motion is at a level of 1 mas yr^{-1} , which can be improved by using QSOs in the near future.

We also compared the measurements in BUL_SC1 made by Sumi, Eyer & Woźniak 2003 (hereafter SC1') with the proper motions presented in this paper, for which our measurements are above the 10σ level of accuracy. The two sets of proper motions for 1368 cross-identified stars are shown

in Fig. 13 together with the best fit line. The offset between the two sets, and the differences between individual measurements are within estimated errors. Note: the scale is different than in Fig. 12. Large reduced chi square in μ_{α} are because Sumi, Eyer & Woźniak 2003 didn't correct systematic distortions (see §3), though their systematic distortions have been reduced at a level of 2 mas yr^{-1} by dividing images into small chunks.

We compared the measurements done by us in one of the overlap regions: between fields BUL_SC1 and BUL_SC45.

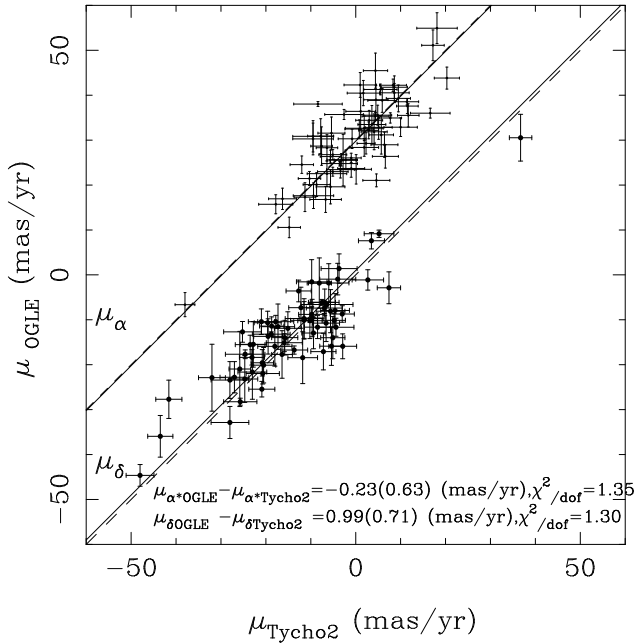


Figure 12. Comparison of proper motions μ_{α^*} (thin) and μ_{δ} (thick) for 65 stars cross-identified in our catalogue and in Tycho-2 catalogue. The proper motions in our catalogue are transformed to the inertial frame by equations (3) and (4). Dashed lines indicate $\mu_{OGLE} = \mu_{Tycho-2}$, and solid lines represent best fit with the offsets: $\mu_{\alpha^*OGLE} - \mu_{\alpha^*Tycho-2} = -0.23 \text{ mas yr}^{-1}$ and $\mu_{\delta OGLE} - \mu_{\delta Tycho-2} = 0.99 \text{ mas yr}^{-1}$. μ_{α^*} are shifted for $+30 \text{ mas yr}^{-1}$ for clarity.

The proper motions of 115 cross-identified stars, and the best fit with a small offset between zero points, are presented in Fig. 14. Here proper motions have been transformed into the inertial frame by equations (3) and (4). Good correlations between them with a rather small zero point offsets: $\mu_{\alpha^*SC1} - \mu_{\alpha^*SC45} = 0.16 \text{ mas yr}^{-1}$ and $\mu_{\delta SC1} - \mu_{\delta SC45} = -0.07 \text{ mas yr}^{-1}$ gives us certain confidence in our measurements and in equations (3) and (4) in terms of the relative the zero point. The scatter is also consistent with the estimated errors.

7 POSSIBLE PROBLEMS

There can be various problems associated with proper motions of variable stars. Our fields are very crowded, hence many stars may be blended. In the case of blending we measure an average position of a blend of several stars within a seeing disk. If a variable star is blended with other stars which have slightly different positions within a seeing disk, the average position of the blended image may change while one component of the blend varies. This change might mimic a proper motion.

As an example we present the time variation of the position of a very long timescale microlensing event candidate (Smith 2003) in the top panel of Fig. 15. The *I*-band light curve of this event is shown in the bottom panel of Fig. 15 (ID=2859 in variable star catalogue of Woźniak et al. 2002). In the top panel we can see an apparent proper motion in the first year which is coincident with the apparent brightness fading, as shown in the bottom panel. After the second year

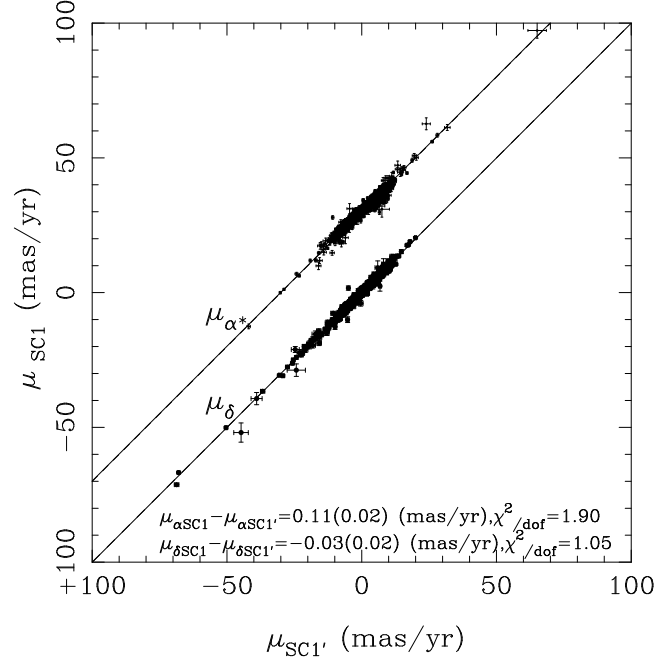


Figure 13. Same figure as Fig. 12 for 1368 stars cross-identified in BUL_SC1 by Sumi, Eyer & Woźniak 2003 (hereafter SC1') and in SC1 by this work, measured with better than 10σ level accuracy. Dashed lines indicate $\mu_{SC1} = \mu_{SC1'}$ which overlap with the solid line in μ_{δ} , and solid lines represent the best fit with the offsets: $\mu_{\alpha^*SC1} - \mu_{\alpha^*SC1'} = 0.11 \text{ mas yr}^{-1}$ and $\mu_{\delta SC1} - \mu_{\delta SC1'} = -0.03 \text{ mas yr}^{-1}$. μ_{α^*} are shifted for $+30 \text{ mas yr}^{-1}$ for clarity. Note: the scale is different from Fig. 12.

the proper motion seems to be small, and the position data points are sparse, which coincides with the low brightness of the star and may reflect the presence of a blend – in poor seeing DoPHOT cannot resolve the two stars, hence there are very few data points in the upper panel. The blend was actually found in the higher resolution OGLE-III images in 2002.

A plausible interpretation is that the microlensed star was brighter than the nearby faint ‘companion’ star in 1997, but by 2000 it became the fainter of the two. The position of the ‘companion’ is consistent with the direction of the apparent proper motion. The faint stars seem to have low proper motion. High resolution observations are needed to fully understand this object.

As another example we present in Fig. 16 the time variation of the position of a star ID=309705 in the OGLE-II field BUL_SC39. Filled circles represent measured positions with type=1 (used in this work), which were at a fixed location for the first three years but moved significantly in the fourth season. The star ID=309705 identified these centroids at the edge of the search radius ($y=-1$) for the first 3 seasons and at the center ($y=0$) in the 4th season. On the other hand, the neighboring star ID=309653 which has a similar brightness of $I = 14.8$ and position of 0.18 pixels East (positive x) and -1.89 pixels South (negative y), identified the same centroids at the edge of the search radius ($y=-1$).

To see the details of this object, in Fig. 16 we also plot the position measurements which are categorized as a star blended with other stars (type=3, which are not used in

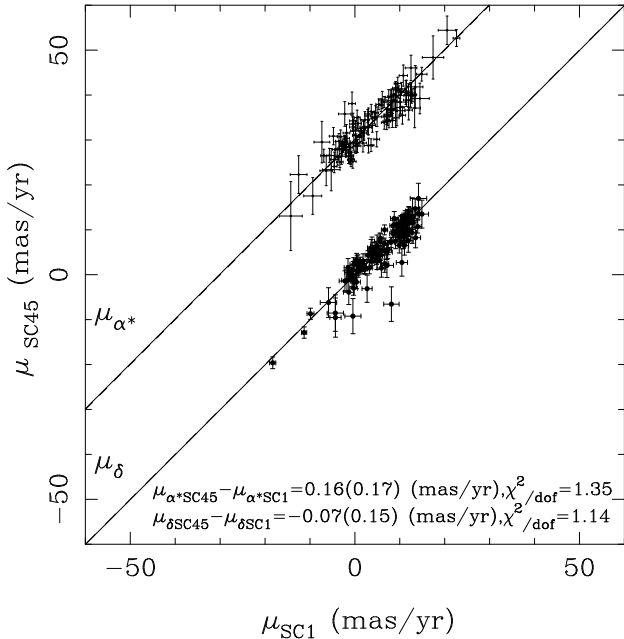


Figure 14. Same figure as Fig. 12 for 115 stars cross-identified in the overlap region between OGLE-II fields BUL_SC1 and BUL_SC45, and measured with better than 5σ level accuracy. Proper motions are transformed into the value in the inertial frame by equations (3) and (4). Dashed lines indicate $\mu_{SC1} = \mu_{SC45}$, and solid lines represent the best fit with the offsets: $\mu_{\alpha^*SC1} - \mu_{\alpha^*SC45} = 0.16 \text{ mas yr}^{-1}$ and $\mu_{\delta SC1} - \mu_{\delta SC45} = -0.07 \text{ mas yr}^{-1}$. μ_{α} in SC45 are shifted for $+30 \text{ mas yr}^{-1}$ for clarity.

this work) by DoPHOT for this star (crosses) and for a neighboring star ID=309653 (dots), which are shifted by $+0.18$ pixels in x and -1.89 pixels in y , i.e. these dots are as they are on the CCD, relative to ID=309705. We can see that these positions (crosses and dots) are identified around $y=0$ (ID=309705) and -2 (ID=309653), respectively, with filled circles in-between them. We also show the I -band light curves of ID=309705 (middle panel) and ID=309653 (bottom panel) in Fig. 16. We can see ID=309705 is constant during four seasons but ID=309653 suddenly faded during the 4th season. This is likely to be a R CrB type variable.

The simplest interpretation is as follows; small number of data points in the seasons 1997-99 indicates that DoPHOT found that object which is composite of these two stars only on the bad seeing frames as a single star with type=1, in other cases they are separated but categorized as blended - type=3. In 2000 when the star ID=309653 faded, the centroid of the composite moved and finally the star ID=309705 became a "single" star with type=1. So the number of data points is large in 2000.

Proper motions of variable stars may have their errors increased not only because of variable contribution of blending, but also because variable stars may change colours, and therefore the coefficient of differential refraction may also change. In rare cases of very long period variables this may be noticeable. Note: we do not treat this kind of objects in a special way, so a reader must be careful when using our catalogue in studies of variable stars.

The effect of blending changes with seeing may contribute to the scatter of data points, but it is not likely to

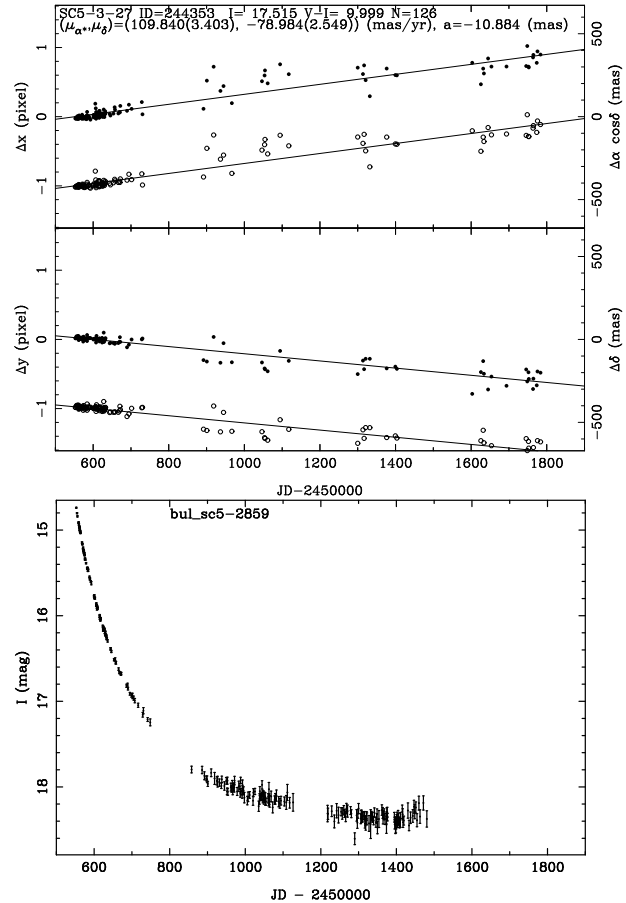


Figure 15. Top panel: Same plots as Fig. 3 for the star ID=244353 in the OGLE-II field BUL_SC5. Filled circles represent actual positions and open circles are correspond to positions corrected for differential refraction, with the offset of -1 pixels. Bottom panel: I -band light curve of same star (ID=2859 in catalogue of Woźniak et al. 2001), a possible very long microlensing event.

have a seasonal effect. Hence, we think that seeing variations are not a major problem.

The probability of blending is much larger for fainter stars, in particular those close to $I = 18$ mag. This may produce a bias in their proper motions, most likely reducing their formal proper motion, as the blended stars may have a different proper motion vector, so the average value is likely to be reduced. We also do not provide a special treatment for this kind of objects, so a reader must be careful when using our catalogue for faint stars.

8 DISCUSSION AND CONCLUSION

We have measured proper motions for 5,080,236 stars in all 49 OGLE-II GB fields, covering a range of $-11^\circ < l < 11^\circ$ and $-6^\circ < b < 3^\circ$. Our catalogue contains objects with proper motions up to $\mu = 500 \text{ mas yr}^{-1}$ and I -band magnitudes in the range $11 \leq I \leq 18$. The accuracy of proper motions in our catalogue is better than 1 mas yr^{-1} for $12 < I < 14$.

One should keep in mind that all measurements of μ presented here are not absolute, but relative to the astrometric reference frame which is roughly that of the Galactic Center (GC) with a small offset seen in the lower panel of Fig. 5. However, as demonstrated in §6, by using the crude estimation for the proper motion of the GC in our reference frame and formula equations (3) and (4), we can obtain crude proper motions in an inertial frame. From the comparison with these inertial values and the Tycho2 catalogue, this transformation seems to work well with errors at a level of 1 mas yr^{-1} . From comparison of μ measured in the overlap region of fields BUL_SC1 and BUL_SC45 (Fig. 14), this transformation works very well in the relative offset from field to field. These zero points for proper motions can be improved by using background quasars which may be detected in the near future using the OGLE-II variability catalogue (Woźniak et al. 2002; Eyer 2002; Dobrzycki et al. 2003).

As demonstrated by Sumi, Eyer & Woźniak (2003), the proper motions based on OGLE-II data can be used to clearly detect the presence of a strong streaming motion (rotation) of stars in the Galactic bar. While the reference frame established from all stars is not well defined with respect to the inertial frame, the relative motions of groups of stars within a given field are well determined.

Though our primary goal is to constrain the Galactic bar model with the future analysis of our catalogue, we provide proper motions for all stars with $I < 18 \text{ mag}$ in all 49 OGLE-II GB fields because this catalogue might be useful for a variety of projects. An analysis of the catalogue is beyond the scope of the present study.

ACKNOWLEDGMENTS

We are grateful to B. Paczyński for helpful comments and discussions. We acknowledge M. Smith for carefully reading the manuscript and helpful comments. We are also thankful to the referee, F. van Leeuwen for suggestive comments. T.S. acknowledge the financial support from the Nishina Memorial Foundation and JSPS. The paper was partly supported by the Polish KBN grant 2P03D02124 to A. Udalski. This work was partly supported with the following grants to B. Paczyński: NSF grants AST-9820314 and AST-0204908, and NASA grants NAG5-12212, and grant HST-AR-09518.01A provided by NASA through a grant from the Space Telescope Science Institute, which is operated by the Association of Universities for Research in Astronomy, Inc., under NASA contract NAS5-26555.

REFERENCES

- Afonso, C. et al. 2003, A&A in press, preprint (astro-ph/0303100)
- Alcock, C. et al. 1997, ApJ, 486, 697
- Alcock, C. et al. 2000a, ApJ, 541, 734
- Aubourg, E. et al. 1993, Nature, 365, 623
- Blitz, L. & Spergel, D. N. S. 1991, ApJ, 379, 631
- Bond, I. A. et al. 2001, MNRAS, 327, 868
- de Vaucouleurs, G. 1964. IAU Symp. 20. The Galaxy and the Magellanic Clouds, ed. F. J. Kerr & A. W. Rogers (Canberra: Australian Acad. Science, MSSSO), 195
- Dehnen, W. & Binney, J. J. 1998, MNRAS, 298, 387
- Dobrzycki, A. et al. 2003, AJ, 125, 1330
- Eisenhauer, F., Schoedel, R., Genzel, R., Ott, T., Tecza, M., Abuter, R., Eckart, A. & Alexander, T., 2003, preprint (astro-ph/0306220)
- Eyer, L. & Woźniak, P. R. 2001, MNRAS, 327, 601
- Eyer, L. 2002, Acta Astronomica, 52, 241
- Gould, A. 1996, PASP, 108, 465
- Häfner, R. et al. 2000, MNRAS, 314, 433
- Høg et al. 2000, A&A, 355, L27
- Kiraga, M., & Paczyński, B. 1994, ApJ, 430, L101
- Kuijken, K. & Rich, R. M. 2002, AJ, 124, 2054
- Mao, S. & Paczyński, B. 2002, preprint (astro-ph/0207131)
- Monet, D. et al. 2002, preprint (astro-ph/0210694)
- Paczynski, B. 1996, ARA&A, 34, 419
- Paczynski, B. & Stanek, K. Z. 1998, ApJ, 494, L219
- Popowski, P. 2003, Invited Review, to appear in "Gravitational Lensing: A Unique Tool For Cosmology", Aussois 2003, eds. D. Valls-Gabaud & J.-P. Kneib (astro-ph/0304464)
- Salim, S. & Gould, A. 2003, ApJ, 582, 1011
- Schechter, L., Mateo, M., & Saha, A. 1993, PASP, 105, 1342S
- Smith, M. C., 2003, MNRAS, 343, 1172
- Spaenhauer, A., Jones, B. F. & Whitford, A. E. 1992, AJ, 103, 297
- Stanek, K. Z. 1996, ApJ, 460, 37L
- Stanek, K. Z. et al. 1994, ApJ, 429, L73
- Stanek, K. Z. et al. 1997, ApJ, 477, 163
- Stanek, K. Z. et al. 2000, Acta Astronomica, 50, 191
- Sumi, T., Eyer, L & Woźniak, P. R. 2003, MNRAS, 340, 1346
- Sumi, T. et al. 2003, ApJ, 591, 204
- Sumi, T. 2003, preprint (astro-ph/0309206)
- Udalski, A. et al. 1993, Acta. Astron., 43, 289
- Udalski, A. et al. 1994, Acta Astronomica, 44, 165
- Udalski, A. et al. 2000, Acta Astronomica, 50, 1
- Udalski, A. et al. 2002, Acta Astronomica, 52, 217
- Udalski, A., Kubiak, M., & Szymański, M. 1997, Acta Astronomica, 74, 319
- Woźniak, P. R., et al. 2001, Acta Astronomica, 51, 175
- Woźniak, P. R., et al. 2002, Acta Astronomica, 52, 129
- Afonso, C. et al. 2003, A&A in press, preprint (astro-ph/0303100)
- Alcock, C. et al. 1997, ApJ, 486, 697
- Alcock, C. et al. 2000a, ApJ, 541, 734
- Aubourg, E. et al. 1993, Nature, 365, 623
- Blitz, L. & Spergel, D. N. S. 1991, ApJ, 379, 631
- Bond, I. A. et al. 2001, MNRAS, 327, 868
- de Vaucouleurs, G. 1964. IAU Symp. 20. The Galaxy and

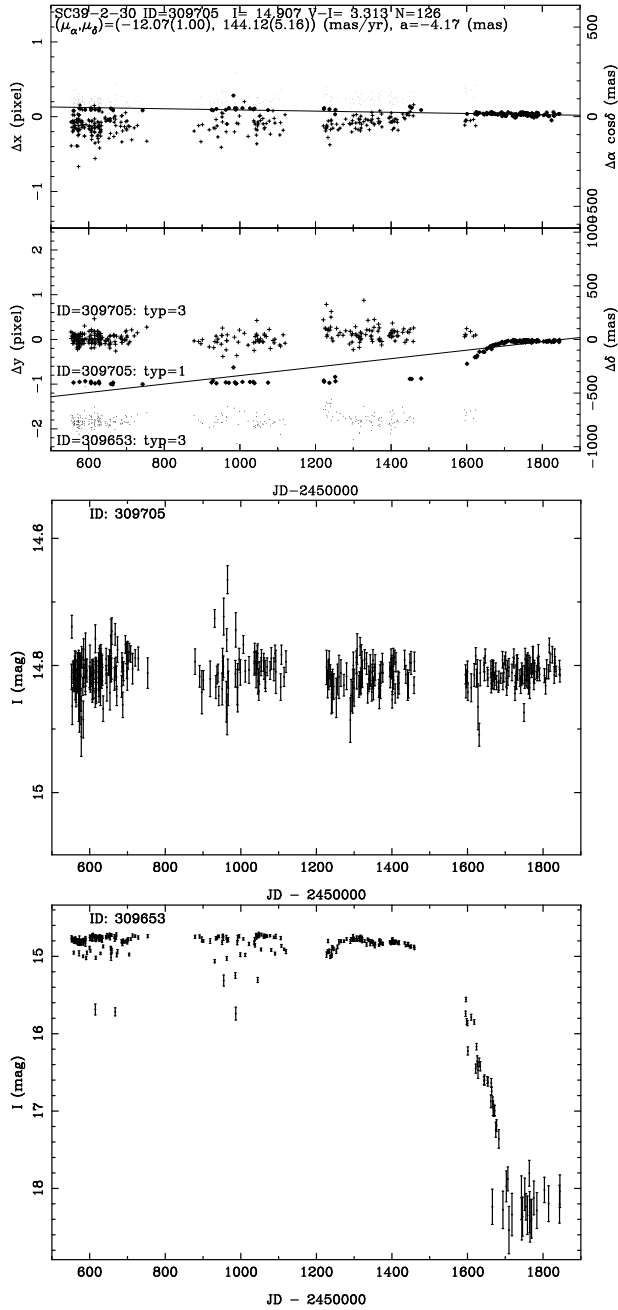


Figure 16. Top: Same plots as Fig. 3 for star ID=309705 in OGLE-II field BUL_SC39. Filled circles represent actual positions with type=1 (used in this work), crosses correspond to position measurements with type=3 (not used) and dots indicate positions measurements of neighboring star ID=309653 with type=3 which are shifted by +0.18 pixels in x and -1.89 pixels in y, i.e. these dots are as they are on CCD, relative to ID=309705. This is a probable case of a blend with one component being a variable star.